Site specific control of crystallographic grain orientation through electron beam additive manufacturing

R. R. Dehoff*[1,2], M. M. Kirka[1,2], W. J. Sames[1,3], H. Bilheux[4], A. S. Tremsin[5], L. E. Lowe[1,2] and S. S. Babu[1,6,7]

Site specific control of the crystallographic orientation of grains within metal components has been unachievable before the advent of metals additive manufacturing (AM) technologies. To demonstrate the capability, the growth of highly misoriented micron scale grains outlining the letters D, O and E, through the thickness of a 25·4 mm tall bulk block comprised of primarily columnar [001] oriented grains made of the nickel base superalloy Inconel 718 was promoted. To accomplish this, electron beam scan strategies were developed based on principles of columnar to equiaxed transitions during solidification. Through changes in scan strategy, the electron beam heat source can rapidly change between point and line heat source modes to promote steady state and/or transient thermal gradients and liquid/solid interface velocity. With this approach, an equiaxed solidification in the regions bounding the letters D, O and E was achieved. The through thickness existence of the equiaxed grain structure outlining the letters within a highly columnar [001] oriented bulk was confirmed through characterizing the bulk specimen with energy selective neutron radiography and confirming with an electron backscatter detection. Ultimately, this demonstration promotes the ability to build metal components with site specific control on crystallographic orientation of grains using the electron beam melting process.

Keywords: Additive manufacturing, Electron beam melting, Grain control, Nickel base superalloy

This paper is part of a special issue on Additive manufacturing

Introduction

The control of crystallographic texture is key to numerous thin film technologies, including microelectronics, transparent conducting films, surface acoustic wave devices and high temperature superconducting wires.[1] Texture is also an important parameter for structural metallic components where crystallographic orientation can significantly influence properties, including elastic modulus, plastic deformation and thermal conductivity. For example, in gas turbine engines, nickel based super alloys are used in single crystal or polycrystalline forms, depending on the desired mechanical properties. Moreover, texture is closely related to grain boundary networks and attempts have been made at grain boundary engineering to control materials behaviour. However, traditional metal part fabrication techniques have limited control to induce site specific grain size and crystallographic orientations due to their inability to control heat transfer conditions at very small length scales. With the emergence of powder bed metal additive manufacturing (AM) techniques, new metallurgical engineering strategies can now be deployed to challenge traditional manufacturing paradigms. This is the central theme of this research paper.

Additive manufacturing with electron beam melting (EBM) uses an electron beam as a heat source to selectively melt successive powder layers to build a three-dimensional component. Currently though, the beam path, or scan strategy, is optimised for specific alloys with the goal of achieving only geometrical accuracy and defect (e.g. porosity) mitigation. Generally ignored has been the *a priori* control of the final microstructure distribution within AM parts by hardware manufacturers.[2,3] Recently though microstructure control within AM processes has become an area of increased interest. Previously published research pertaining to

[1]Manufacturing Demonstration Facility, Oak Ridge National Laboratory, Oak Ridge, TN, USA
[2]Materials Science & Technology Division, Oak Ridge National Laboratory, Oak Ridge, TN, USA
[3]Department of Nuclear Engineering, Texas A&M University, College Station, TX, USA
[4]Chemical and Engineering Materials Division, Oak Ridge National Laboratory, Oak Ridge, TN, USA
[5]Space Sciences Laboratory, University of California at Berkeley, Berkeley, CA, USA
[6]Energy and Transportation Science Division, Oak Ridge National Laboratory, Oak Ridge, TN, USA
[7]Department of Mechanical, Aerospace and Biomedical Engineering, The University of Tennessee, Knoxville, TN, USA

*Corresponding author, email dehoffrr@ornl.gov

© 2015 Institute of Materials, Minerals and Mining
Published by Maney on behalf of the Institute
Received 13 October 2015; accepted 27 November 2014
DOI 10.1179/1743284714Y.0000000734

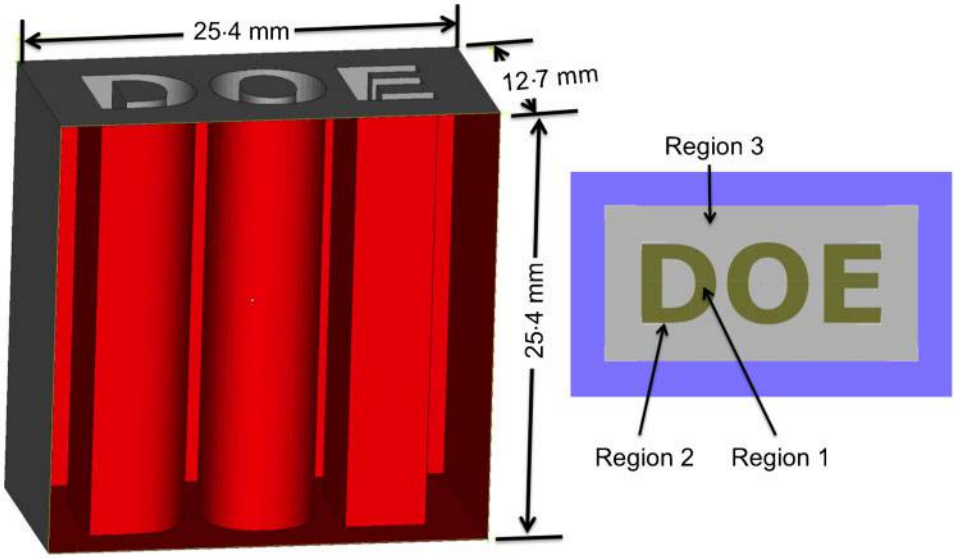

1 Computer aided design file showing alphabets DOE and delineation of three regions within letters for engineering of crystallographic grain orientation, i.e. Region 1: mixed mode that is combination of columnar and equiaxed growth mode; Region 2: highly misoriented equiaxed grain growth; Region 3: <001> columnar grain growth

microstructure control during a laser AM process focused on process modelling and identification of process parameter windows to ensure the formation of epitaxial growth throughout added layers during the repair of high value single crystal nickel base (Ni base) superalloy components.[4] Körner *et al.*[5] has shown recently the potential for forming either epitaxial or equiaxed structures through variations of scan strategy in the Arcam EBM process for Inconel 718. Additionally, Antonysamy *et al.*[6] has studied the effects of part thickness on the resultant grain structure in association with contour and bulk melt scans in thin walled Ti–6Al–4V parts made using the Arcam EBM process. However, to achieve targeted architectured microstructures, within a given metallic component, the ability to dynamically switch between equiaxed and columnar solidification conditions on demand, i.e. *a priori*, without extensive trial and error experimentation, is needed and is something that has not been demonstrated in a controlled manner to date.

In this work, a beam scanning strategy to spatially control both the ultimate part shape and to simultaneously impose predetermined spatial three-dimensional crystallographic grain orientation patterns through multiple layers was attempted. The strategy dynamically adjusts the melt pool shape, size, temperature gradient (G, K m^{-1}) and liquid/solid interface velocity (R, m s^{-1}), while maintaining the external/internal geometry imposed by a computer aided design file. This was made possible through precise manipulation of the electron beam current (I) and electron beam velocity (v) guided by analytical models of heat transfer.

Experimental methods

Demonstration samples were fabricated using rotary atomised powder of the Ni base superalloy Inconel 718; the chemical composition is given in Table 1. The size distribution of the powder particles was in the mesh size range from −100 to +325 (44–149 μm). The EBM process was performed within an Arcam A2 system, using EBM Control software version 4.1.22. Fifty micron thick layers were used for the part, and each layer was preheated and postheated in accordance with the commercially available melting themes for Inconel 718. To demonstrate control of the local grain structure, a rectangular block of dimensions 25·4 × 25·4 × 12·7 mm was built which contained the letters D, O and E through the entire thickness of the block as shown in Fig. 1*a*. To delineate the letters from the bulk, three regions were designed to have grains with different crystallographic orientations (Fig. 1*b*) and assigned specific EBM parameters (discussed below) to alter the G and R. Although simplistic, this experimental design demonstrates both straight and curvilinear geometrical features typical to that of components made by additive manufacturing.

To provide guidance in choosing EBM melt parameters to produce controlled spatial variation of G and R, analytical models for fusion welding compiled by Grong[7] were used. Poignantly, these calculations are to be considered as approximate representation of dynamic process that is characteristic to EBM. Typical calculations such as below were used to guide the beam scan strategies outlined in Fig. 2, such that the local solidification conditions were sufficient to traverse the columnar and equiaxed solidification modes. For example, the equation for describing the temperature as a function of x, y, z and time for steady state condition is given below

$$T = T_0 + \frac{\eta Q/V}{2\pi\lambda/[t(t+t_0)]^{1/2}} \exp\left\{-\frac{1}{4a}\left[\frac{(z+z_0)^2}{t} + \frac{y^2}{t+t_0}\right]\right\} \quad (1)$$

Table 1 Nominal chemical composition of Inconel 718 powder

Element	Ni	Fe	Cr	Mo	Nb	Ti	Al	Co	Mn	Cu	Si	C
Content/wt-%	Bal.	18·2	18·2	3	5	1	0·5	0·1	0·1	0·05	0·2	0·05 (max.)

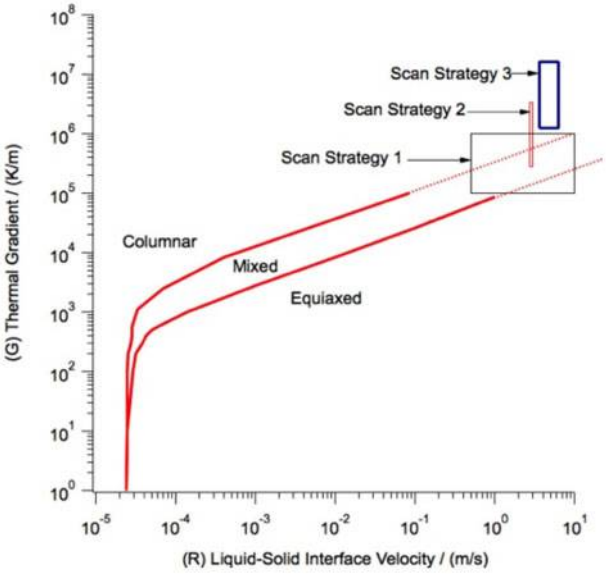

2 Solidification map for Inconel 718 with estimated ranges for *G* and *R* for each of scan strategies overlaid[30]

In the above equation, T_0 is the preheat temperature (for Inconel 718, the preheat temperature is 1273 K), Q is the net heat input in Joules (efficiency × voltage × current), V is the welding velocity, λ is thermal conductivity, t is the time, y is the distance along the width of the powder bed and z is the distance along thickness powder bed. Furthermore, a is thermal diffusivity, t_0 is given by $(r_b^2/4a)$ and r_b is the radius of the heat source (200 μm). z_0 is defined as $[(r_b/e)(\pi a r_b/V)]^{0\cdot5}$. Using physical parameters for solid nickel, typical thermal profiles were estimated for different parameters for typical scan strategies. At lower scanning speeds (Fig. 3*a*), the melt pool shape is typical that of fusion welding showing an ellipsoid shape. However, with an increase in scanning speeds (Fig. 3*b* and *c*), the melt pool shapes start resembling a liner melt pool shape. These changes are estimated to produce large variations in G and R within a given layer during additive manufacturing corresponding to regions 1–3.

Using the above analytical modelling as a guide, the derived processing parameters for each of the three unique regions are given in Table 2 with the intended solidification conditions (G and R) indicated in Fig. 2. The line melting strategy used in Region 3 utilised a continuous snake raster. The spot melting strategies used had the same nominal beam parameters, but the order of when each spot was melted was changed using Arcam algorithms. This order dictates the amount of time that each spot has to cool down, before an adjacent spot being melted. Additionally, the order of melting of the bulk and spot regions was different. The order of melting for each layer progressed with (1) Region 2, (2) Region 3 and (3) Region 1. This affects the local thermal conditions of the material before the spot melting.

To characterise the EBM deposit, both energy selective neutron radiography and electron backscatter diffraction (EBSD) were used. The energy selective neutron radiography was used to confirm the through thickness characteristics of the letters D, O and E and EBSD to confirm the neutron imaging results. A 5 mm thick piece of the block taken from the centre was imaged with a VULCAN engineering diffractometer at the spallation neutron source. For transmission imaging experiments, a microchannel detector was installed close to the sample position and was timed to measure neutron pulses as they arrived.[31] The neutron position and wavelength were recorded in each radiograph at a spatial resolution of 150 μm (~10 times coarser than EBSD) and a time resolution up to 10 μs. Data were collected at 60 Hz, the clock at which the spallation neutron source operates, for an overall time of 2 h.

With spallation neutron sources, neutrons of all wavelengths are travelling in pulses through the beamline optics during a very short pulse. Short wavelength neutrons are detected first at the sample position. Longer wavelength neutrons arrive later within the same pulse. The wavelength λ or energy E of the neutrons can be determined by time of flight (TOF)

$$\lambda = \frac{h(t-t_e)}{m_n L};\ E = \frac{h^2 m_n^2}{4\pi^2\lambda^2} \tag{2}$$

where t is the time of detection, t_e is the time of emission, m_n is the mass of a neutron and L is the distance between the source and the detector. According to Bragg's law, neutrons can be diffracted when

$$\lambda_{hkl} = 2d_{hkl}\sin\theta_{hkl} \tag{3}$$

where d_{hkl} is the interplanar distance for the (hkl) planes and θ_{hkl} is the angle between the incident neutron beam and the crystal plane. As illustrated in Fig. 4, when the crystalline lattice planes are aligned with the incident neutron beam, i.e. $\theta_{hkl}=90°$, neutrons backscattered towards the neutron source. For a longer neutron wavelength (i.e. $\theta_{hkl}>90°$), there is no diffraction and the neutron beam transmits through the lattices. The neutron transmission increases abruptly at a wavelength $\lambda_{Bragg\ edge}$, displaying the so called Bragg edge. For a shorter neutron wavelength ($\theta_{hkl}<90°$), the incident beam is scattered with a deviation $2\theta_{hkl}$.

Thus, the neutron radiograph acquired at a given energy can provide spatial variation of the number of crystals having any of their (hkl) direction making an angle β_{hkl}, with the incident beam such that $\beta_{hkl}=(\pi/2)-\arcsin(\lambda_{hkl}/2d_{hkl})$. At $\lambda=\lambda_{Bragg\ edge}=2d_{hkl}$, $\beta_{hkl}=90°$. Similarly to diffraction, the position of the Bragg edges in the spectrum is characteristic to the crystal structure. A shifted Bragg edge corresponds to a change in the lattice spacing, i.e. strain, for planes perpendicular to the incident neutron beam. This novel technique called Bragg edge imaging enables studies of crystallographic properties (strain, texture and phase) in a non-destructive *in*

Table 2 EBM process parameters for melt strategies used

Region	Scan strategy	Current/mA	Focus offset/mA	Max current/mA	Speed/mm s^{-1}	Speed function	Spot time/ms
3 (Bulk)	Line	15	3	21	4530	98	N/A
2 (Boundary)	Spot	10	3	10	800	30	1·3
1 (Letters)	Spot	10	3	10	800	30	1·3

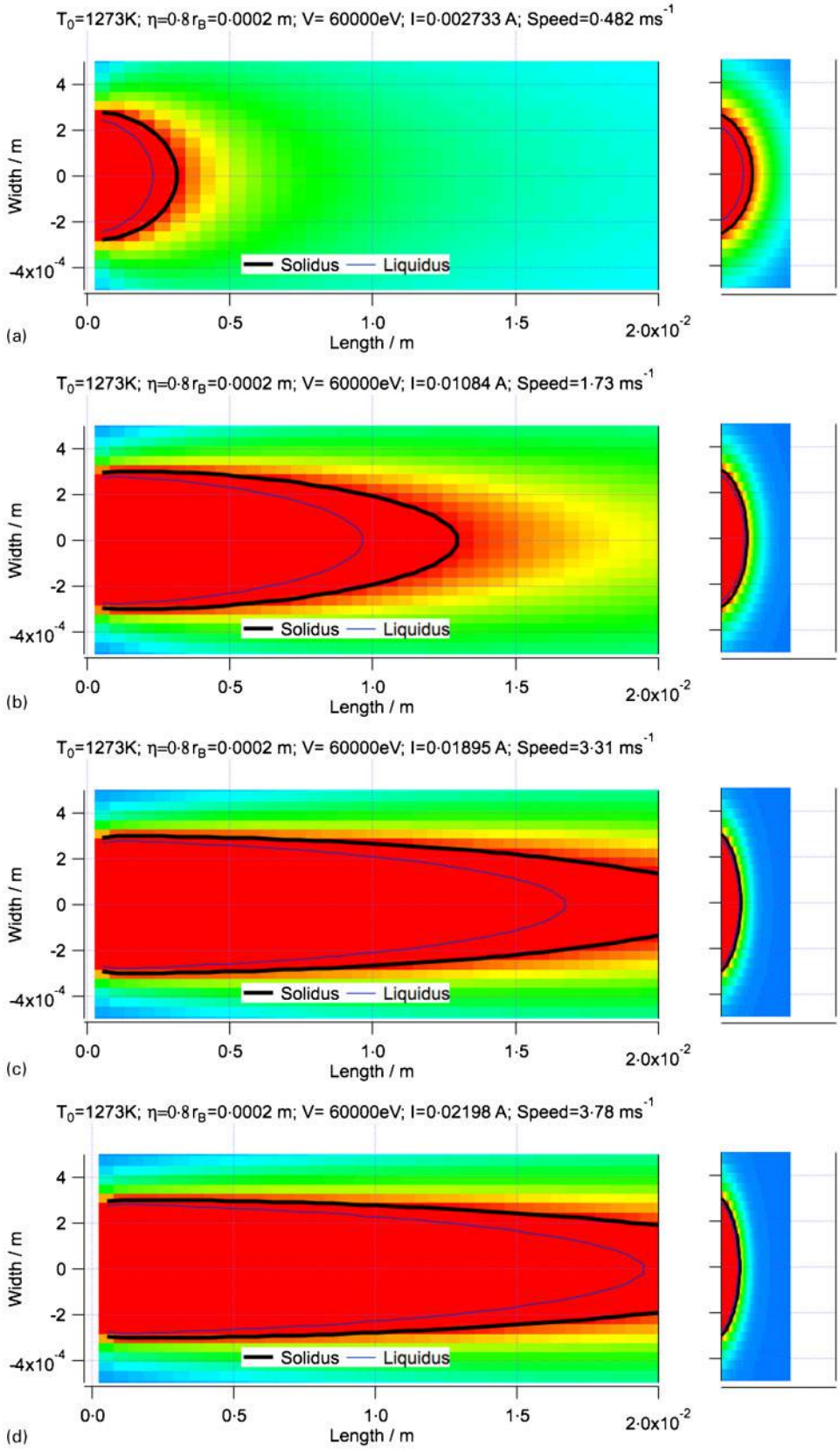

a Beam current=2·733mA and Scan velocity=0·482 m/s *b* Beam current=10·84mA and Scan velocity=1·73m/s *c* Beam current=18·95mA and Scan velocity=3·31 m/s and *d* Beam current=21·98mA and Scan velocity=3·78 m/s.

3 Calculated weld pool shape (top view and cross-section view) from Inconel 718 alloys using equation (1) for various electron beam currents and scanning speeds that is accessible during the EBM process. With increasing electron beam scan speed, the melt pool shape becomes shallow and elongated, giving rise to a [001] crystallographic growth preference from (n-1)th layer into nth layer. Depth of cross-section view is 200 μm; with increasing welding speed, melt pool shape becomes shallow and elongated and would prefer <001> crystallographic growth from (n−1)th layer into nth layer

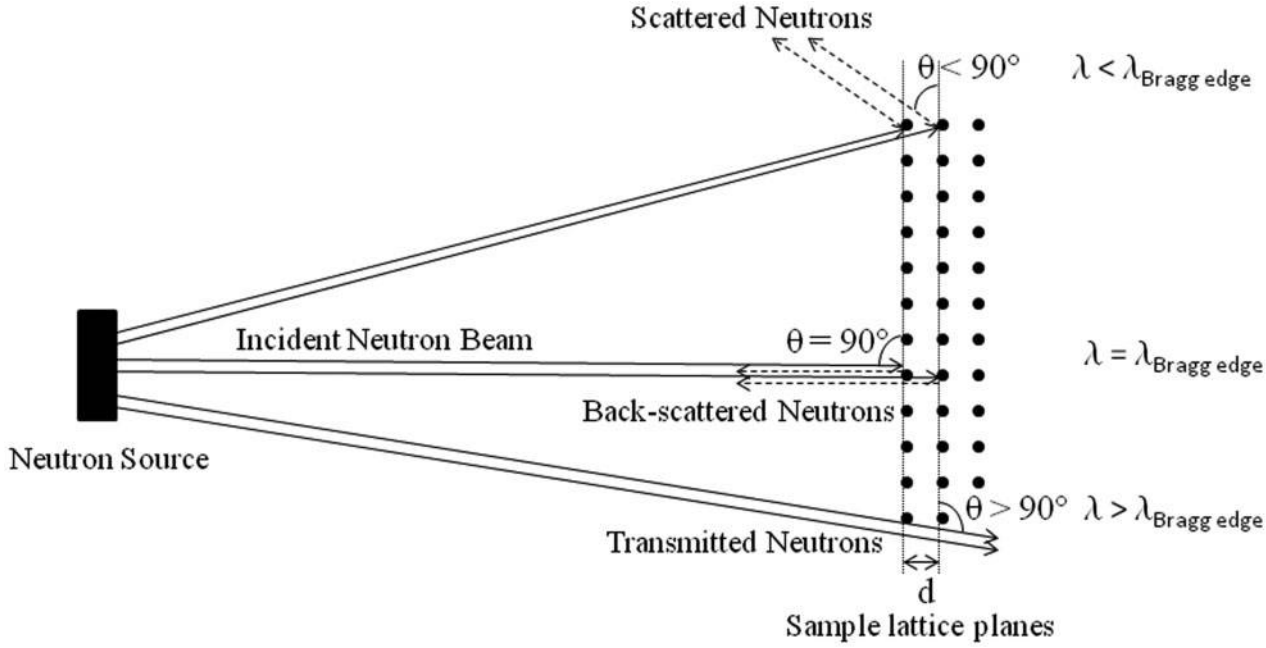

4 Schematic of neutron interaction with lattice planes of crystalline structure as function of scattering angle θ_{hkl}: (top) for specific neutron wavelength λ, shorter than Bragg edge wavelength $\lambda_{Bragg\ edge}$, incident neutron beam enters crystalline lattice with $\theta<90°$ and is scattered with deviation of 2θ; (centre) lattice planes are aligned with incident neutron, i.e. $\theta=90°$, which backscattered towards neutron source; (bottom) for neutron wavelength longer than Bragg edge wavelength, there is no diffraction and neutron beam can transmit; in this figure, *d* is distance between lattice planes and θ is scattering angle

situ measurement. In the case of spallation neutron sources, the angle between the incident neutron beam and the lattice planes is fixed; the neutron wavelength λ varies, as a function of time (see above TOF technique).

After neutron radiography, the surface of the 5 mm thick piece was characterised through EBSD on a Philips XL30 FEG SEM, using a TSL/EDAX Hikari camera. The accelerating voltage was 20 kV, spot size was 5 and the step size was 10 μm. The scan was 25 230 by 11 800 μm for a total of 2 980 844 data points.

Results and discussion

Electron beam current and velocity are a function of x, y and layer (z) coordinates, which can be used to control microstructure and part geometries. These two parameters primarily influence directional solidification[8–12] that dictates the transition from columnar to equiaxed transition as a function of G and R. Such solidification maps for Inconel 718 have been predicted using the classic theory of Hunt[13] and extensions of that theory.[14] The second set of information is the minimum and maximum values of G and R as a function of process parameters. In this regard, we used pre-existing knowledge of weld modelling published by Grong.[7] Through the established welding theory, ranges for G and R for the different scan strategies relevant to the EBM process were estimated. These calculations and other welding research suggest the possibility to achieve wide ranges of G and R within a single melt region by changing the amount of energy imparted as a function of time.[15,16] On the other hand, constant G and R values can be achieved in a steady state weld pool shape that is moving at a constant velocity.[17] It is important to note that the spatial and temporal process parameter (I and v) ranges for these transitions will depend on the required local area of grain control.

Modelling suggested that transitions between columnar to equiaxed solidifications in the regions shown in Fig. 2, can be induced by switching between point and line heat sources. Shown in Fig. 5*a* is the 5 mm thick section of the Inconel 718 sample used for energy selective neutron radiography characterisation with the letters D, O and E not visible from the outside. The neutron radiograph shown in Fig. 5*b* provides access to grain orientation through the thickness of the sample with differences in neutron transmission due to the Bragg edge scattering at specific wavelengths. The letters D, O and E are observed with a mixture of <001> columnar oriented and equiaxed crystalline structure indicated by the change in grey (darker areas are oriented differently than brighter areas). In contrast, the areas surrounding the letters are textured with a preferred <001> grain orientation throughout the thickness of the sample. The <001> orientation is inferred from the fact that neutrons preferentially transmit through in the brighter areas and neutrons are diffracted in the darker areas. The crystallographic textures that define the letter contours result in contrasting neutron transmission, due to inhomogeneous Bragg scattering from the distinct textures of the different regions. A movie file of the images obtained different wavelengths is provided in Supplementary Material 1 http://dx.doi.org/10.1179/1743284714Y.0000000734.s1.

The EBSD results confirming the through thickness results from neutron tomography are shown in Fig. 6. The misorientation map shows that preferred <001> columnar solidification grain growth dominates in Region 3 (Figs. 5*b* and 6). This is expected because, in this region, a standard EBM line scan strategy (Scan Strategy 3) was used which causes partial remelting of

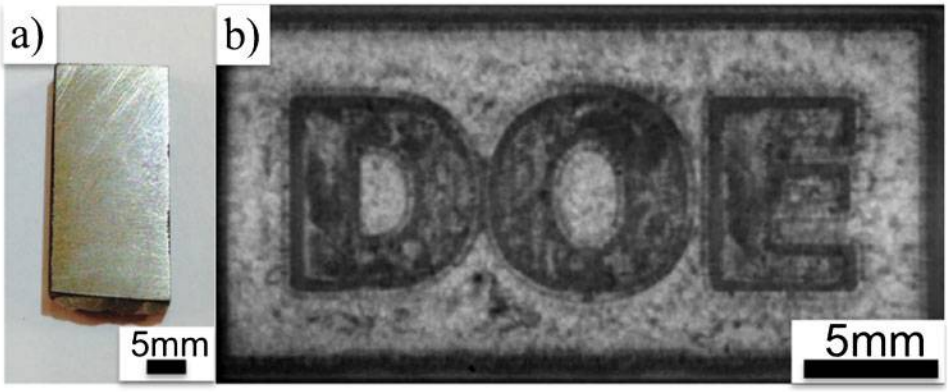

5 *a* photograph and *b* energy selective neutron radiograph of 5 mm Inconel 718 sample taken from within interior of larger 25·4 mm thick specimen made with AM techniques: neutron radiograph was measured at spallation neutron source VULCAN engineering diffractometer using thermal neutrons at wavelength of 1·5 Å, with spatial resolution of 150 μm

the grains in the previous layer and results in epitaxial growth of grains into the current layer. This behaviour has been widely reported by researchers in field of AM of metals.[18,19] However, in Region 2, the point melt scan strategies (Scan Strategy 2) impose G and R that are at the boundary of transition from columnar to equiaxed solidification growth. As expected through the design approach, this region demonstrates extensive misoriented growth with reference to Region 3 (thus, the contrast observed in Fig. 5*b*). Furthermore, in Region 1, point heat transfer conditions (Scan Strategy 1) were imposed to achieve dynamic variations of G and R, which will induce oscillations across the columnar and equiaxed transition zones, as observed in Fig. 5*b*. Although, equal distribution of <001> columnar and misoriented growth were expected, only 10–20% equiaxed grains were observe. This can be related to transient variations of G and R with reference to transient melt pool shapes in Region 1.

Admittedly, small volumes within each of the regions were found to deviate from the intended design. Hypothesised is that these regions are associated with stochastic variations of G and R during the rapid changes in beam positions imposed by the scanning strategies. Such stochastic variations in grain structure are also seen in AM gas turbine airfoil repair processes that desire only single crystal grain growth and even in single crystal casting where stray grain formation causes a significant number of casting to be rejected.[4,20–22] However, irrespective of these few areas of unexpected grain orientations, the above results confirmed the hypothesis that controlled crystallographic texture in a tailored fashion could be achieved by manipulating heat transfer conditions in an electron beam powder bed additive manufacturing process.

Overall, the role of G and R on the solidification grain orientation is well known. For example, Park *et al.*[23] demonstrated that, for a given temperature gradient in a

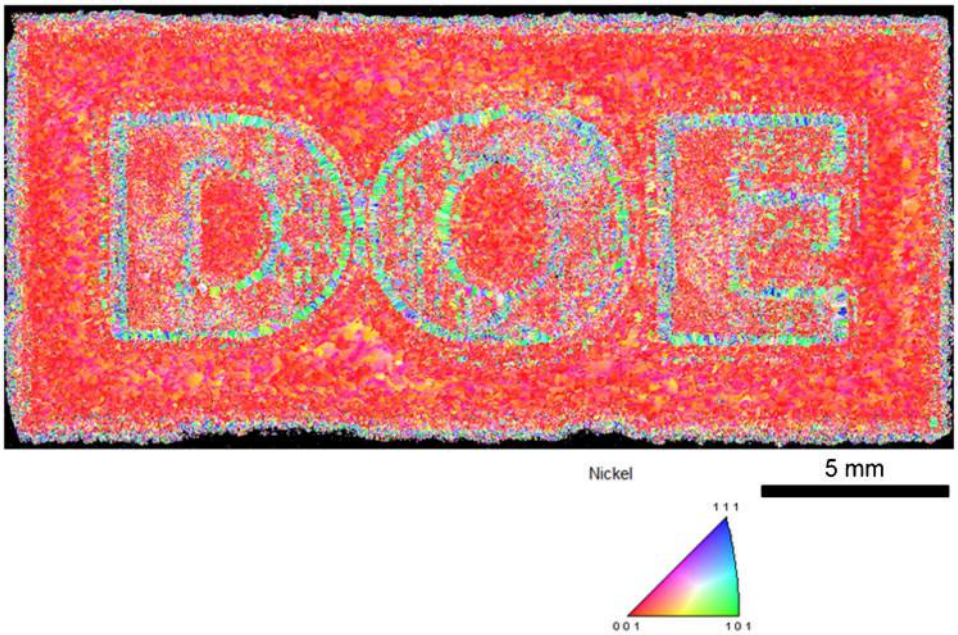

6 Crystallographic orientation map corresponding to inverse pole figure for fcc nickel obtained on cross-section of EBM build obtained through EBSD: as intended, Region 1 shows preferred <001> columnar solidification grain growth; similarly, Region 2 shows misoriented growth indicated by lack of any significant <001> components; lastly, Region 3 shows interior areas of letters D, O and E with mixture of <001> growth and misoriented growth

steady state welding conditions, large variations in crystallographic texture can be achieved by changing the dendrite growth velocity. Rappaz *et al.*[17] have developed an elegant geometric model that predicts the spatial variation of G and R for a given weld pool shape. This model has been validated for a wide range of welding conditions. Using these geometrical models, researchers have estimated the probability of stray grains during welding processes.[24] However, the referenced welding experiments were all performed under steady state heat transfer conditions and therefore, no attempt was made to control the evolution of the microstructure.

For AM processes, analysis of G versus R and the resulting microstructures is also common. Bulk columnar structures in Inconel 718 have been confirmed (using standard raster scan strategies) in EBM[25] and laser melting.[26] Work on Ti–6Al–4V has shown the ability to obtain columnar structures exhibiting high degrees of misorientation between the grains in the bulk structure.[27] Work in AlSi10Mg shows high misorientation (and growth direction) of columnar grains in the bulk material, which is directly traceable to the individual melt pool solidification.[28] Other work shows that the modification of scan strategy in laser melting to reduce residual stress through 'island scanning' can have interesting, and unintended, consequences on grain orientation. As a result of 'island scanning', a repetitive structure develops throughout the bulk material that is associable with the scan pattern.[29]

Heat transfer and fluid modelling have been extensively employed in studying the epitaxial laser metal forming and scanning laser epitaxy processes for use in the repair of polycrystalline and single crystal gas turbine airfoils.[4,21] However, the primary aim of these processes has been to promote either wholly columnar or equiaxed grain growth.[4,20,21] Furthermore, in the particular case of the selective laser epitaxy process, the process is designed only to melt a single 1–2 mm thick layer of material onto to an existing base substrate of the desired crystallographic texture (equiaxed or single crystal) and not build bulk compoennts.[20,21] A recent study on Ti–6Al–4V structures considered the impact of fine equiaxed grain nucleation due to unmelted powder in the contour scan region and the related importance of part thickness on the size of grains in thin walled structures in EBM.[6] Ultimately, nevertheless, the effort was not directed towards interlayer microstructure control. Very recently, efforts on Inconel 718 have sought to control the columnar to equiaxed transition in parts made using the Arcam EBM process through increasing or decreasing the speed of the electron beam.[5] However, with the particular approach methodology adopted in the previous efforts,[5] dynamic changes of process parameters to allow for transitions between epitaxial and equiaxed grain growth and back are not possible due to constraints in the equipment.

Although previous researchers have observed columnar to equiaxed transitions and attempted to control the resultant microstructure in welding and AM processes, the direction has always been towards having a part wholly comprised of a single microstructure, either equiaxed or columnar grains. Through this work has been demonstrated the ability to control G and R spatially on a micron scale, while achieving the desired grain orientation spatially within a given layer throughout the entire thickness of the par. This is a novelty previously not reported.

Conclusions

Analytical modelling has been used as a guide to design EBM scan strategies, for spatial and temporal control over thermal gradient and liquid/solid interface stability, to provide interlayer crystallographic texture control and subsequently, achieve bulk parts with a desired spatial texture. This control was achieved by rapidly hopping between the point to line heat source mode, as well as, steady and transient states. This approach was successfully demonstrated on a Ni base superalloy Inconel 718, where the letters D, O and E were outlined by highly misoriented equiaxed grain structure through the thickness of a bulk part that has oriented [001] columnar structure. Confirmation of through thickness presence of these grain orientations was confirmed through non-destructive energy - resolved radiography of the part and EBSD imaging of metallographic surfaces. While few regions did deviate from the intended crystallographic design, the deviations can be attributable to transient thermal gradients existing within the melt pool. Ultimately, this approach provides a fundamentally new design tool that empowers the fabrication of microstructure tailored components with any arbitrary geometries.

Acknowledgements

Research is sponsored by the US Department of Energy, Office of Energy Efficiency and Renewable Energy, Advanced Manufacturing Office, under contract DE-AC05-00OR22725 with UT-Battelle, LLC. The research conducted at the spallation neutron source was sponsored by the Scientific User Facility Division, Office of Basic Energy Sciences, US Department of Energy. This research was also supported by fellowship funding received from the US Department of Energy, Office of Nuclear Energy, Nuclear Energy University Programs. The United States Government retains and the publisher, by accepting the article for publication, acknowledges that the United States Government retains a non-exclusive, paid-up, irrevocable, worldwide license to publish or reproduce the published form of this manuscript, or allow others to do so, for United States Government purposes.

References

1. G. K. Lewis and E. Schlienger: 'Practical considerations and capabilities for laser assisted direct metal deposition', *Mater. Des.*, 2000, **21**, 417–423.
2. Y. Tian, D. McAllister, H. Colijn, M. Mills, D. Farson, M. Nordin and S. Babu: 'Rationalization of microstructure heterogeneity in Inconel 718 builds made by the direct laser additive manufacturing process', *Metall. Mater. Trans. A*, 2014, **45A**, 4470–4483.
3. S. Suwas and R. Ray: 'Crystallographic texture of materials', 1st edn; 2014, London, Springer.
4. M. Gäumann, S. Henry, F. Cleton, J. D. Wagniere and W. Kurz: 'Epitaxial laser metal forming: analysis of microstructure formation', *Mater. Sci. Eng. A*, 1999, **A271**, 232–241.
5. C. Körner, H. Helmer, A. Bauereiß and R. F. Singer: 'Tailoring the grain structure of IN718 during selective electron beam melting', *MATEC Web Conf.*, 2014, **14**, 08001.
6. A. Antonysamy, J. Meyer and P. Prangnell: 'Effect of build geometry on the β-grain structure and texture in additive

manufacture of Ti6Al4V by selective electron beam melting', *Mater. Charact.*, 2013, **84**, 153–168.
7. O. Grong: 'Metallurgical modeling of welding' 2nd edn; 1997; London, Institute of Materials.
8. R. Trivedi and W. Kurz: 'Dendritic growth', *Int. Mater. Rev.*, 1994, **39**, 49–74
9. W. J. Boettinger, S. R. Coriell, A. L. Greer, A. Karma, W. Kurz, M. Rappaz and R. Trivedi: 'Solidification microstructures: recent developments, future directions', *Acta Mater.*, 2000, **48**, 43–70.
10. W. Kurz, B. Giovanola and R. Trivedi: 'Theory of microstructural development during rapid solidification', *Acta Metall.*, 1986, **34**, 823–830.
11. S. A. David and J. M. Vitek: 'Correlation between solidification parameters and weld microstructures', *Int. Mater. Rev.*, 1989, **34**, 213–245.
12. S. A. David and T. DebRoy: 'Current issues and problems in welding science', *Science*, 1992, **257**, 497–502.
13. J. D. Hunt: 'Steady state columnar and equiaxed growth of dendrites and eutectic', *Mater. Sci. Eng.*, 1984, **65**, 75–83.
14. M. Gäumann, C. Bezençon, P. Canalis and W. Kurz: 'Single-crystal laser deposition of superalloys: processing–microstructure maps', *Acta Mater.*, 2001, **49**, 1051–1062.
15. S. S. Babu, J. W. Elmer, J. M. Vitek and S. A. David: 'Time-resolved X-ray diffraction investigation of primary weld solidification in Fe–C–Al–Mn steel welds', *Acta Mater.*, 2002, **50**, 4763–4781.
16. T. Zacharia, S. A. David, J. M. Vitek and H. G. Kraus: 'Computational modeling of stationary gas tungsten-arc weld pools and comparison to stainless steel 304 experimental results', *Metall. Mater. Trans. B*, 1991, **22B**, 243–257.
17. M. Rappaz, S. A. David, J. M. Vitek and L. A. Boatner: 'Analysis of solidification microstructures in Fe–Ni–Cr single-crystal welds', *Metall. Mater. Trans. A*, 1990, **21A**, 1767–1782.
18. L. E. Murr, S. M. Gaytan, D. A. Ramirez, E. Martinez, J. Hernandez, K. N. Amato, P. W. Shindo, F. R. Medina and R. B. Wicker: 'Metal Fabrication by additive manufacturing using laser and electron beam melting technologies', *J. Mater. Sci. Technol.*, 2012, **28**, 1–14.
19. D. A. Ramirez, L. E. Murr, E. Martinez, D. H. Hernandez, J. L. Martinez, B. I. Machado, F. Medina, P. Frigola and R. B. Wicker: 'Novel precipitate–microstructural architecture developed in the fabrication of solid copper components by additive manufacturing using electron beam melting', *Acta Mater.*, 2011, **59**, 4088–4099.
20. R. Acharya, R. Bansal, J. Gambone and S. Das: 'A coupled thermal, fluid flow, and solidification model for the processing of single-crystal alloy CMSX-4 through scanning laser epitaxy for turbine engine hot-section component repair (part I)', *Metall. Mater. Trans. B*, 2014, doi: 10·1007/s11663-014-0117-9.
21. M. Kirka, R. Bansal and S. Das: 'Recent progress on scanning laser epitaxy: A new technique for growing single crystal superalloys', Proc. 20th Solid Freeform Fabrication Symp., Austin, TX, USA, August 2009, University of Texas, 799–806.
22. R. Reed: 'The superalloys fundamentals and applications', 1st edn; 2006, London, Cambridge University Press.
23. J. W. Park, J. M. Vitek, S. S. Babu and S. A. David: 'Stray grain formation, thermomechanical stress and solidification cracking in single crystal nickel base superalloy welds', *Sci. Technol. Weld. Join.*, 2004, **9**, 472–482.
24. J. M. Vitek: 'The effect of welding conditions on stray grain formation in single crystal welds — theoretical analysis', *Acta Mater.*, 2005, **53**, 53–67.
25. A. Strondl, S. Milenkovic, A. Schneider, U. Klement and G. Frommeyer: 'Effect of processing on microstructure and physical properties of three nickel-based superalloys with different hardening mechanisms', *Adv. Eng. Mater.*, 2012, **14**, 427–438.
26. K. N. Amato, S. M. Gaytan, L. E. Murr, E. Martinez, P. W. Shindo, J. Hernandez, S. Collins and F. Medina: 'Microstructures and mechanical behavior of Inconel 718 fabricated by selective laser melting', *Acta Mater.*, 2012, **60**, 2229–2239.
27. S. S. Al-Bermani, M. L. Blackmore, W. Zhang and I. Todd: 'The origin of microstructural diversity, texture, and mechanical properties in electron beam melted Ti–6Al–4V', *Metall. Mater. Trans. A*, 2010, **41A**, 3422–3434.
28. L. Thijs, K. Kempen, J.-P. Kruth and J. van Humbeeck: 'Fine-structured aluminum products with controllable texture by selective laser melting of pre-alloyed AlSi10Mg powder', *Acta Mater.*, 2013, **61**, 1809–1819.
29. L. N. Carter, C. Martin, P. J. Withers and M. M. Attallah: 'The influence of the laser scan strategy on grain structure and cracking behavior in SLM powder-bed fabricated nickel superalloy', *J. Alloys Compd*, 2014, **615**, 338–347.
30. L. Nastac, J. J. Valencia, M. L. Tims and F. R. Dax: 'Advances in the solidification of IN718 and RS5 Alloys', Proceedings of Superalloys 718, 625, 706 and Various Derivatives, Ed. E. A. Lora, TMS, 2001.
31. A. S. Tremsin, J. B. McPhate, A. Steuwer, W. Kockelmann, A. M. Paradowska, J. F. Kelleher, J. V. Vallerga, O. H. W. Siegmund and W. B. Feller: 'High-resolution strain mapping through time-of-flight neutron transmission diffraction with a microchannel plate neutron counting detector', *Strain*, 2012, **48**, 296–305.